Coverage Analysis for Millimeter Wave Cellular Networks With Imperfect Beam Alignment

Ming Cheng, *Student Member, IEEE*, Jun-Bo Wang, *Member, IEEE*, Yongpeng Wu, *Senior Member, IEEE*,
Xiang-Gen Xia, *Fellow, IEEE*, Kai-Kit Wong, *Fellow, IEEE*, and Min Lin, *Member, IEEE*

***Abstract*—Millimeter wave (mmWave) communications is a promising approach to satisfy the increasing high data rate requirement of next generation mobile communications. This paper studies the downlink coverage performance of mmWave cellular networks with imperfect beam alignment. An enhanced antenna model is adopted to model the directional antenna beamforming pattern, in which the mainlobe beamwidth and directivity gain can be expressed as functions of the number of elements in the antenna array. After deriving the probability density function of the distance between mobile station and its serving base station (BS), the directivity gain with imperfect beam alignment is obtained as a discrete random variable. Then, a computationally tractable expression is obtained for the coverage probability of mmWave cellular networks. This generalized expression can be applied in different blockage regimes, e.g., general blockage regime, full-blockage regime, and nonblockage regime with or without beam alignment errors. Numerical results show that small beam alignment errors will not deteriorate the coverage performance significantly, and the antenna array with the less number of elements provides higher robustness against the beam alignment errors. Moreover, when the beam alignment error is small enough, the coverage performance can be improved by increasing the BS intensity and the number of elements in the antenna array.**

***Index Terms*—Millimeter wave (mmWave), coverage probability, beam alignment errors, enhanced antenna model, stochastic geometry.**

I. Introduction

WITH the fast development of portable devices and the explosive growth of internet applications, mobile communications have become indispensable in our daily life. One of the main characteristics of future mobile networks is the unprecedented traffic volumes [1]. To cope with the exponentially increasing demands for high data rate wireless accesses, several key technologies have been proposed [2], [3]. In particular, millimeter wave (mmWave) communications is widely considered as one of the most important technologies to achieve 10 Gbit/s peak date rate. So far, many efforts have been devoted to the research of mmWave communications [4], [5]. Several standards have been defined for indoor wireless personal area networks or wireless local area networks (WLANs) in the mmWave bands, such as ECMA-387 [6], IEEE 802.15.3c [7], and IEEE 802.11ad [8].

Compared to the sub-6 GHz signal utilized in conventional cellular networks, the mmWave signal has wider bandwidth and smaller wavelength. Since expanding the bandwidth is an effective and efficient approach to increase the system throughput, mmWave communications is considered as one of the most important technologies to offer orders of magnitude increases in cellular capacity. Moreover, the small wavelength of mmWave signals enables large antenna arrays to be placed in a compact size, which can provide high gains and directivities. Although the wide bands of mmWave signals potentially offer significant performance improvements in wireless networks, the high frequencies also introduce challenges when applying mmWave in cellular networks. According to the Friis transmission law [5], the power of received signal decreases with the increase of the signal frequency. The mmWave signals will experience severe path loss during propagation. As a result, the communication range of mmWave is about 200 meters or less [5], which is a normal size of microcells in mobile networks. Moreover, the frequency relevant rain attenuation and atmospheric absorption also increase the path loss, which further shortens the communication range [9]. In order to expand the communication distance and improve the signal quality, antenna arrays with directional beamforming, which can provide directivity gain to compensate for the additional path loss, are often deployed at both transmitters and receivers. How to measure the performance gains of beamforming is a hot topic for mmWave communications.

The system performance of mmWave communications has been studied in numerous existing works. Understanding the

Manuscript received December 19, 2017; revised March 19, 2018 and May 10, 2018; accepted May 20, 2018. Date of publication May 31, 2018; date of current version September 17, 2018. This work was supported in part by the National Nature Science Foundation of China under Grants 61720106003, 61571115, and 61602235, in part by the European Union's Horizon 2020 research and innovation programme under the Marie Skłodowska-Curie Grant agreement 709291, and in part by the Natural Science Foundation of Jiangsu Province of China (BK20161007). The review of this paper was coordinated by Prof. D. B. da Costa. *(Corresponding authors: Jun-Bo Wang and Ming Cheng.)*

M. Cheng and J.-B. Wang are with National Mobile Communications Research Laboratory, Southeast University, Nanjing 210096, China (e-mail: mingcheng@seu.edu.cn; jbwang@seu.edu.cn).

Y. Wu is with the Shanghai Key Laboratory of Navigation and Location Based Services, Shanghai Jiao Tong University, Minhang 200240, China (e-mail: yongpeng.wu@sjtu.edu.cn).

X.-G. Xia is with the Department of Electrical and Computer Engineering, University of Delaware, Newark, DE 19716 USA (e-mail: xxia@ee.udel.edu).

K.-K. Wong is with the Department of Electronic and Electrical Engineering, University College London, London WC1E 6BT, U.K. (e-mail: kai-kit.wong@ucl.ac.uk).

M. Lin is with the Key Lab of Broadband Wireless Communication and Sensor Network Technology, Ministry of Education, Nanjing University of Posts and Telecommunications, Nanjing 210003, China (e-mail: linmin@njupt.edu.cn).

Color versions of one or more of the figures in this paper are available online at http://ieeexplore.ieee.org.

Digital Object Identifier 10.1109/TVT.2018.2842213

propagation of mmWave signals is vital for the design and performance evaluation of mmWave systems. In [10], [11], the channel measurements were conducted using directional antenna arrays. The results showed that the mmWave signals suffer from severe penetration loss when they pass through common materials such as concrete and bricks, which causes substantial difference between the line-of-sight (LOS) propagation paths and the non-line-of-sight (NLOS) propagation paths. In [12], by using the measurements of mmWave outdoor cellular propagation in New York City, the statistical channel models were derived for outage analysis of mmWave systems. However, such works based on simulations and measurements are costly and time-consuming. In addition, the results are only valid for the particular scenario and may not be applicable to more diverse propagation environments.

Owing to the mathematical flexibility of stochastic geometry [13], system performance metrics of conventional cellular networks, such as coverage probability and average rate, can be derived in computationally tractable forms by modeling the locations of base stations (BSs) as a stochastic point process, for example Poisson point process (PPP) [14]. There are also several applications of stochastic geometry to study mmWave networks, such as analysis of coverage and capacity performance in cellular mmWave networks [15]–[18] and in ad hoc mmWave networks [19], [20]. It should be noted that all studies in [15]–[20] characterized the impacts of beamforming of antenna arrays based on the flat-top model. The sinc and cosine antenna models and the antenna array response were used to analyze the impacts of antenna array size and BSs co-operations on coverage performance in [21] and [22], respectively. Unfortunately, since the antenna models in [21] and [22] were too complicated, the analyses were limited to the scenarios in which each mobile station (MS) is assumed to be equipped with only one single antenna. Moreover, the analyses in [15]–[22] assumed the beam alignment to be perfect which is impossible for practical systems. With imperfect beam alignment, the ergodic capacity for mmWave ad hoc networks and the coverage probability and average rate for multi-tier mmWave cellular networks were analyzed in [23] and [24], respectively. However, the analytical expression for the ergodic capacity loss due to imperfect beam alignment in [23] was only valid in the high signal-to-interference-and-noise ratio (SINR) regime, and the analysis in [24] was conducted by simplifying the states of propagation links with the two-ball approximation. Moreover, the size of the antenna arrays has not been taken into account in [23] or [24].

In summary, for mmWave networks where both BS and MSs are equipped with multiple antennas, there is no comprehensive investigation on the impact of the size of antenna arrays on the system performance when beam alignment errors exist. To analyze the system coverage performance with different sizes of antenna arrays, the model of antenna array should be able to depict the performance characteristics, such as directivity gains and beamwidths, with the number of elements in antenna arrays accurately and directly. The model should also be tractable enough to obtain the system performance in analytical expression. Moreover, when beam alignment errors occur, the actual power gains of antenna arrays and the impact on the system performance should be analyzed exactly. Motivated by these requirements, our prior work in [25] proposed an enhanced directional beamforming model to analyze the downlink coverage probability of mmWave networks with imperfect beam alignment. We incorporated random factors such as blockage, number of elements in the antenna array, and beam alignment errors, and the coverage probability was carried out in an analytical expression. Compared with our prior work in [25], this paper improves the enhanced directional beamforming model, provides a generalized mathematical framework using stochastic geometry, and includes the detailed mathematical derivations. The coverage probabilities in special cases such as extreme blockage environments and perfect beam alignment are also analyzed. Moreover, the impact of BS intensity is demonstrated by numerical results in this paper as well. The main contributions are summarized as follows:

- Enhanced flat-top model for directional antenna beamforming. Using the antenna theory, this paper adopts a more realistic enhanced flat-top model into the analysis of coverage performance of mmWave networks. In our enhanced flat-top model, the mainlobe beamwidth and directivity gains of antenna arrays can be characterized as functions of the number of elements in the antenna array.
- Directivity gains with beam alignment errors. With the enhanced flat-top model, the alignment is achieved when the azimuth of target transmitter or receiver falls in the mainlobe of its antenna array. Assuming the beam alignment error follows a truncated Gaussian distribution, the alignment probability is obtained. Then, the directivity gain with imperfect beam alignment is derived as a discrete distributed random variable.
- Analytical expression for downlink coverage probability. By modeling the BSs as two independent non-homogeneous PPPs, this paper takes the BS location randomness and blockage effects into account. With the enhanced flat-top antenna model and the derived directivity gain distribution, an analytical expression of downlink coverage probability is derived for mmWave cellular networks. The derived analytical expression is computationally tractable. Our generalized expression can be applied in different blockage regimes with and without beam alignment errors. The coverage in [15] can be a special case of our analysis.
- Impacts of the number of elements in the antenna array and the imperfect beam alignment. The obtained analytical expression reveals the impacts of the number of elements in the antenna array and the imperfect beam alignment on the coverage probability. When the beam alignment errors are small enough, increasing the number of elements in the antenna array can improve the coverage performance. However, when the beam alignment errors are large, increasing the number of elements in the antenna array will decrease the coverage probability severely.

The rest of this paper is organized as follows. The system model is introduced in Section II. In Section III, after deriving the probability density function (PDF) of distance between MS and its serving BS and the directivity gains of antenna arrays with imperfect beam alignment, the downlink coverage probability is obtained in a computationally tractable form. Numerical results are presented in Section IV, and conclusions are drawn in Section V.

II. System Model

A. Network Model

Consider a mmWave cellular network where all BSs are arranged according to a two dimensional homogenous PPP Φ with intensity λ. MSs are distributed as a stationary point process independent to the BSs. A typical MS, denoted as MS_0, is assumed to be located at the origin o. All signals are transmitted using the mmWave bands. Compared to the lower-frequency bands, the signals on the mmWave bands are more sensitive to blockage effects in the propagation. The blockages cause substantial differences in the LOS and NLOS path loss characteristics. The propagation path between BS and MS can be LOS or NLOS. Mathematically, the probability of being an LOS propagation path [26] is

$$\mathbb{P}_{\mathrm{LOS}}\left(r\right) = e^{-\beta r} \tag{1}$$

where β is the blockage parameter determined by the density and average size of the blockages, and r is the distance between the BS and the MS. Accordingly, the probability of a propagation path being NLOS is

$$\mathbb{P}_{\mathrm{NLOS}}\left(r\right) = 1 - \mathbb{P}_{\mathrm{LOS}}\left(r\right) = 1 - e^{-\beta r}. \tag{2}$$

The LOS probabilities are assumed to be independent for different BSs.

All BSs can be divided into two independent[1] non-homogenous PPPs based on their propagation paths to MS_0. They are the LOS BS process Φ_{L} with intensity function $\lambda\mathbb{P}_{\mathrm{LOS}}\left(r\right)$ and the NLOS BS process Φ_{N} with intensity function $\lambda\mathbb{P}_{\mathrm{NLOS}}\left(r\right)$. Furthermore, MS_0 is served by the BS, either LOS or NLOS, which provides the strongest average received power. The serving BS is denoted as BS_0. In other words, the propagation path between MS_0 and BS_0 has the smallest path loss.

B. Channel Model

The LOS and NLOS propagation paths will have different path loss exponents, α_{L} and α_{N}, respectively. Typical values of mmWave path loss exponents are available in [11]. In general, they satisfy $\alpha_{\mathrm{N}} > \alpha_{\mathrm{L}} > 0$. Referring to [15], if the length of the propagation path between BS and MS is r, the path loss $l\left(r\right)$ can be calculated as

$$l\left(r\right) = l_{\mathrm{L}}\left(r\right)\mathbb{1}_{\mathrm{LOS}} + l_{\mathrm{N}}\left(r\right)\mathbb{1}_{\mathrm{NLOS}} \tag{3}$$

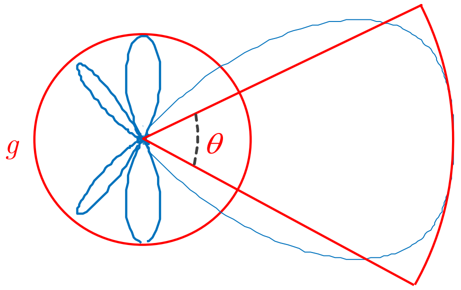

Fig. 1. Directional beamforming antenna model.

where $\mathbb{1}_{\mathrm{LOS}}$ $(\mathbb{1}_{\mathrm{NLOS}})$ is the Dirichlet function which is one when the BS is LOS (NLOS). $l_{\mathrm{L}}\left(r\right)$ and $l_{\mathrm{N}}\left(r\right)$ are path loss functions for LOS propagation path and NLOS propagation path, respectively. The two path loss functions are further assumed to be

$$l_{\mathrm{L}}\left(r\right) = \left(1+r\right)^{-\alpha_{\mathrm{L}}} \tag{4}$$

and

$$l_{\mathrm{N}}\left(r\right) = \left(1+r\right)^{-\alpha_{\mathrm{N}}}, \tag{5}$$

respectively[2].

Measurements show that the small scale fading has a relatively minor impact on mmWave cellular systems [5]. Moreover, due to the poor scattering environment, the Rayleigh fading model for the sub-6 GHz bands, which is predicated on a large amount of local scattering, does not apply in principle for mmWave bands, especially when directional beamforming is applied [5]. In this paper, as in [15], [21] and [27], the small scale fading on each propagation path is assumed to be independent Nakagami distributed. Then the power fading h is a normalized Gamma random variable and its PDF is expressed as

$$f_h\left(x\right) = \frac{m^m}{\Gamma\left(m\right)}x^{m-1}e^{-mx}, \quad x > 0 \tag{6}$$

where $\Gamma\left(\cdot\right)$ is the Gamma function, and m is the Nakagami parameter. For the LOS and NLOS propagation paths, m is set to be N_{L} and N_{N}, respectively. For the tractability of the following analysis, N_{L} and N_{N} are assumed to be positive integers [15].

C. Enhanced Directional Beamforming Model

In order to compensate for the frequency dependent path-loss, antenna arrays are assumed to be deployed at both the BSs and MSs to perform directional beamforming. To maintain the analytical tractability, the flat-top model is often used to characterize the pattern of the directional beamforming, which is shown in Fig. 1, where G is the mainlobe directivity gain, g is the sidelobe directivity gain and θ is the beamwidth of the mainlobe [15], [28]. In conventional flat-top model, the main performance parameters of antenna arrays, such as G, g, θ, are idealistic, and the relation between these parameters and the antenna array physical implementation, such as the number of elements in the antenna array, is not given.

In this paper, antenna arrays deployed at both BSs and MSs are assumed to be uniform linear antenna arrays (ULAs) and

---

[1] Note that because of the correlations of blockage effects among propagation paths, the LOS probabilities for different propagation paths are not independent in reality. However, ignoring such correlations causes a minor loss of accuracy. In this paper, we ignore the correlations of blockage effects and assume the LOS probabilities are independent. By the independent LOS probabilities assumption, the LOS BSs and NLOS BSs form two independent point processes.

[2] 1 is introduced to ensure that the path loss function is always less than 1.

we adopt a more realistic flat-top antenna model to depict the antenna radiation patterns. According to [29], for a ULA with N antenna elements, if the maximum radiation intensity $U_{\max}$ is normalized to be one, the average intensity is approximated by

$$U_0 \approx \frac{\pi}{Nkd} = \frac{\lambda_c}{2Nd} \tag{7}$$

where λ_c is the wavelength, $k = 2\pi/\lambda_c$ is the wave number, and d is the antenna element separation. To avoid the grating lobes, the maximum element separation should be less than half-wavelength, i.e., $d < \lambda_c/2$. Meanwhile, the half-power beamwidth (HPBW) can be expressed as [29]

$$\theta_{\mathrm{H}} \simeq 2\left[\frac{\pi}{2} - \cos^{-1}\left(\frac{1.391\lambda_c}{\pi N d}\right)\right], \quad \pi d/\lambda_c \ll 1. \tag{8}$$

If the antenna element separation is set to be $d = \rho\lambda_c$ and $\rho < 1/2$, the radiation intensities and HPBW will be functions of the number of elements N in the antenna array. Using (8), the mainlobe beamwidth in the flat-top model can be derived as

$$\theta\left(N\right) = \theta_{\mathrm{H}} = \pi - 2\cos^{-1}\left(\frac{1.391}{\pi\rho N}\right). \tag{9}$$

If the mainlobe gain is assumed to be the maximum radiation intensity, i.e.,

$$G = U_{\max} = 1, \tag{10}$$

the sidelobe gain g will be a function of N given by

$$\begin{aligned} g\left(N\right) &= \frac{2\pi U_0 - \theta\left(N\right)U_{\max}}{2\pi - \theta\left(N\right)} \\ &= \frac{\pi/(\rho N) - \pi + 2\cos^{-1}(1.391/(\pi\rho N))}{\pi + 2\cos^{-1}(1.391/(\pi\rho N))} \end{aligned} \tag{11}$$

From (9) and (11), ρN can be treated as a single factor, which means that antenna arrays with the same ρN value have the same performance parameters. Fig. 2 shows the performance parameters of antenna array with different numbers of elements given ρ. It can be seen that both the mainlobe beamwidth and the sidelobe gain decrease with the increase of the number of elements in the antenna array. Moreover, the antenna array with $\rho = 1/4$ and $N = N_1$ has the same performance parameters as the antenna array with $\rho = 1/8$ and $N = 2N_1$.

D. Beam Alignment Error Model

In order to receive the most desired signal power, both the MS and its serving BS will estimate the angles of arrival (AoAs) and angles of departure (AoDs), respectively, and then adjust their antenna steering orientations to exploit the maximum directivity gain. The multiple signal classification (MUSIC) algorithm in [30] and the auxiliary beam pair (ABP) design based estimation algorithm in [31] have been employed for the mmWave band. However, the practical limitations, such as the errors in the AoA and AoD estimations, the antenna array perturbations due to the position errors of the antenna elements, and the mutual coupling between antenna elements, will cause the antenna array point away from the desired target [32]. In this paper, the beam alignment error δ is modeled as a truncated-Gaussian distributed variable with zero mean [23], whose PDF is

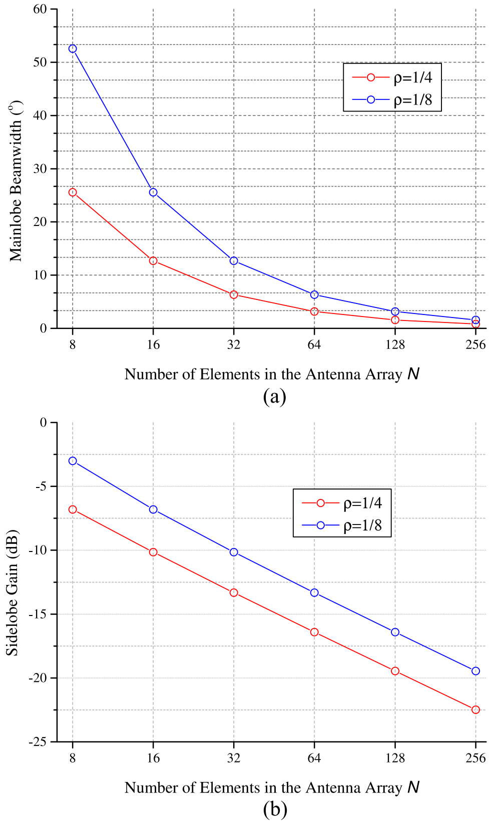

Fig. 2. Performance of antenna array with different numbers of elements. (a) Mainlobe beamwidth. (b) Sidelobe gain.

TABLE I
ABSOLUTE BEAM ALIGNMENT ERROR AND STANDARD DEVIATION

$\lvert\delta\rvert$	0°	1°	2°	3°	4°	5°
σ	0	0.0219	0.0437	0.0656	0.0875	0.1094

$$f_\delta\left(t\right) = \frac{\sqrt{\frac{2}{\pi\sigma^2}}e^{-\frac{t^2}{2\sigma^2}}}{\mathrm{erf}\left(\frac{\pi}{\sqrt{2}\sigma}\right) - \mathrm{erf}\left(\frac{-\pi}{\sqrt{2}\sigma}\right)}, \quad t \in (-\pi, \pi] \tag{12}$$

where $\mathrm{erf}\left(x\right) = 2\int_0^x e^{-t^2}\mathrm{d}t \Big/ \sqrt{\pi}$ is the error function, and σ is the standard deviation of the original Gaussian variable. Furthermore, the expectation of the absolute error $|\delta|$ can be calculated by

$$\mathbb{E}\left[|\delta|\right] = \frac{2\sqrt{2}\sigma}{\mathrm{erf}\left(\frac{\pi}{\sqrt{2}\sigma}\right) - \mathrm{erf}\left(\frac{-\pi}{\sqrt{2}\sigma}\right)}\frac{1}{\sqrt{\pi}}\left(1 - e^{-\frac{\pi^2}{2\sigma^2}}\right). \tag{13}$$

According to (13), $|\delta|$ is a monotonically increasing function of σ, as shown in Table I.

III. DOWNLINK COVERAGE ANALYSIS

This section will analyze the coverage probability of the proposed mmWave cellular networks. First, the PDF of the distance between MS_0 and its serving BS, either LOS or NLOS, is provided. Then, the directivity gains with imperfect beam alignment are analyzed. Finally, the coverage of the mmWave cellular networks is obtained in a computationally tractable expression.

In this paper, all BSs are assumed to serve MSs with the same power. Mathematically, the coverage probability P_c is defined as the probability that the signal to interference and noise ratio (SINR) at MS_0 side is larger than some threshold T, i.e.,

$$P_\mathrm{c} \triangleq \mathbb{P}\left[\mathrm{SINR} > T\right]. \tag{14}$$

In (14), the received SINR can be expressed as

$$\begin{aligned}\mathrm{SINR} &\triangleq \frac{h_0 m_{\mathrm{R}_0} m_{\mathrm{T}_0} l\left(r_0\right)}{\sum_{i\in\Phi\backslash\{0\}} h_i m_{\mathrm{R}_i} m_{\mathrm{T}_i} l\left(r_i\right) + \sigma_n^2}\\ &= \frac{h_0 m_{\mathrm{R}_0} m_{\mathrm{T}_0} l\left(r_0\right)}{I_\mathrm{L} + I_\mathrm{N} + \sigma_n^2}\end{aligned} \tag{15}$$

where h_0 is the power fading on the desired propagation path, and σ_n^2 is the thermal noise power normalized by the transmit power, m_{R_0} (m_{R_i}) is the directivity gain of receiving antenna array at MS_0 for the desired (interfering) signal, m_{T_0} (m_{T_i}) is the directivity gain of transmitting antenna array at the serving BS_0 (the interfering BS_i), and r_0 (r_i) is the distance between MS_0 and BS_0 (BS_i). In (15), I_L is the aggregate interference from all the other LOS BSs (except the serving BS for MS_0) in Φ_L and can be expressed as

$$I_\mathrm{L} = \sum_{i\in\Phi_\mathrm{L}\backslash\{0\}} h_{\mathrm{L}_i} m_{\mathrm{R}_i} m_{\mathrm{T}_i} l_\mathrm{L}\left(r_i\right) \tag{16}$$

where h_{L_i} is the power fading on the propagation path between MS_0 and interfering LOS BS BS_i. Similarly, I_N is the aggregate interference from all the other NLOS BSs (except the serving BS for MS_0) in Φ_N and can be expressed as

$$I_\mathrm{N} = \sum_{i\in\Phi_\mathrm{N}\backslash\{0\}} h_{\mathrm{N}_i} m_{\mathrm{R}_i} m_{\mathrm{T}_i} l_\mathrm{N}\left(r_i\right) \tag{17}$$

where h_{N_i} is the power fading on the propagation path between MS_0 and interfering NLOS BS BS_i.

A. PDF of Distance Between MS_0 *and* BS_0

Let r_L (r_N) be the distance between MS_0 and its nearest LOS (NLOS) BS. If the serving BS of MS_0 is LOS, the path loss satisfies

$$l_\mathrm{L}\left(r_\mathrm{L}\right) > l_\mathrm{N}\left(r_N\right) \tag{18}$$

which can be derived as

$$r_\mathrm{N} > \left(1 + r_\mathrm{L}\right)^{\alpha_\mathrm{L}/\alpha_\mathrm{N}} - 1. \tag{19}$$

Similarly, if the serving BS of MS_0 is an NLOS one, we have

$$r_\mathrm{L} > \left(1 + r_\mathrm{N}\right)^{\alpha_\mathrm{N}/\alpha_\mathrm{L}} - 1. \tag{20}$$

To facilitate the following analysis, two functions are defined as follows

$$\psi_\mathrm{L}\left(r\right) = \left(1 + r\right)^{\alpha_\mathrm{L}/\alpha_\mathrm{N}} - 1, \tag{21}$$

$$\psi_\mathrm{N}\left(r\right) = \left(1 + r\right)^{\alpha_\mathrm{N}/\alpha_\mathrm{L}} - 1. \tag{22}$$

Lemma 1: If MS_0 is associated with an LOS BS, the PDF of the distance to its serving BS is expressed in (23), shown at the bottom of this page. In contrast, if MS_0 is associated with an NLOS BS, the PDF of the distance to its serving BS is expressed in (24), shown at the bottom of this page.

Proof: The proof is given in Appendix A. ■

B. Directivity Gains With Imperfect Beam Alignment

Based on the enhanced flat-top beamforming model, the alignment is achieved when the azimuth of target transmitter or receiver falls in the mainlobe of its antenna array. In other words, if the absolute beam alignment error is not larger than half of the mainlobe beamwidth, i.e., $|\delta| \leq \theta\left(N\right)/2$, the antenna array is deemed to be aligned. Using (12), the alignment probability can be calculated by

$$\begin{aligned}\mathbb{P}_\mathrm{A}\left(\sigma, N\right) &= \mathbb{P}\left[|\delta| \leq \frac{\theta\left(N\right)}{2}\right]\\ &= \frac{\mathrm{erf}\left(\frac{\pi - 2\cos^{-1}\left(\frac{1.391}{\pi\rho N}\right)}{2\sqrt{2}\sigma}\right)}{\mathrm{erf}\left(\frac{\pi}{\sqrt{2}\sigma}\right)}.\end{aligned} \tag{25}$$

It can be observed from (25) that the alignment probability changes with ρ, N, and σ. Moreover, antenna arrays with the same ρN value have the same alignment performance. Fig. 3 shows the alignment probability versus the number of elements in the antenna array with different alignment errors. It can be known from Fig. 3 that the alignment probability decreases with the increase of the number of elements in the antenna array and the beam alignment error.

Since the beam alignment is not perfect, the directivity gain of the receiving (transmitting) antenna array for the desired signal of MS_0, m_{R_0} (m_{T_0}), can be described as a discrete random variable. Moreover, the probability mass functions (PMFs) of m_{R_0} and m_{T_0} can be expressed as

$$f_{m_{\mathrm{R}_0}}\left(x\right) = \begin{cases} \mathbb{P}_\mathrm{A}\left(\sigma_\mathrm{R}, N_\mathrm{R}\right) & x = 1\\ 1 - \mathbb{P}_\mathrm{A}\left(\sigma_\mathrm{R}, N_\mathrm{R}\right) & x = g\left(N_\mathrm{R}\right)\end{cases} \tag{26}$$

$$f_\mathrm{L}\left(x\right) = 2\pi\lambda x \mathbb{P}_\mathrm{LOS}\left(x\right)\exp\left(-2\pi\lambda\left(\int_0^x t\mathbb{P}_\mathrm{LOS}\left(t\right)\mathrm{d}t + \int_0^{\psi_\mathrm{L}\left(x\right)} t\mathbb{P}_\mathrm{NLOS}\left(t\right)\mathrm{d}t\right)\right), x > 0 \tag{23}$$

$$f_\mathrm{N}\left(x\right) = 2\pi\lambda x \mathbb{P}_\mathrm{NLOS}\left(x\right)\exp\left(-2\pi\lambda\left(\int_0^x t\mathbb{P}_\mathrm{NLOS}\left(t\right)\mathrm{d}t + \int_0^{\psi_\mathrm{N}\left(x\right)} t\mathbb{P}_\mathrm{LOS}\left(t\right)\mathrm{d}t\right)\right), x > 0 \tag{24}$$

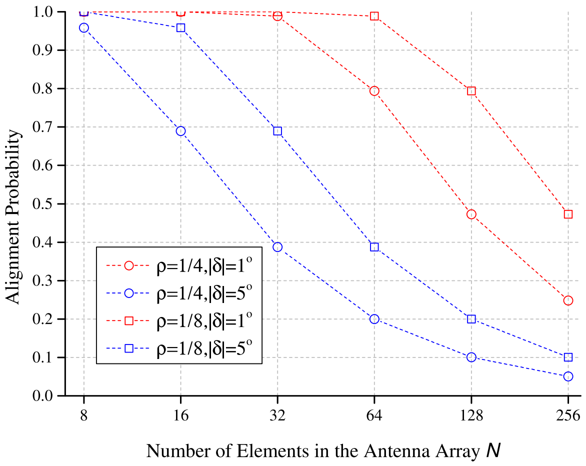

Fig. 3. Alignment probability with the number of elements in the antenna array.

and

$$f_{m_{\mathrm{T}_0}}(x) = \begin{cases} \mathbb{P}_{\mathrm{A}}(\sigma_{\mathrm{T}}, N_{\mathrm{T}}) & x = 1 \\ 1 - \mathbb{P}_{\mathrm{A}}(\sigma_{\mathrm{T}}, N_{\mathrm{T}}) & x = g(N_{\mathrm{T}}) \end{cases}, \tag{27}$$

respectively, where N_{R} (N_{T}) and σ_{R} (σ_{T}) are the number of elements in the antenna array and the beam alignment error standard deviation of the receiving (transmitting) antenna array at MSs (BSs), respectively. Meanwhile, if both the AoAs and AoDs of interfering propagation paths are assumed to be independently and uniformly distributed in $(-\pi, \pi]$, the PMFs of directivity gains of the receiving and transmitting antenna arrays for interfering signals of MS_0, m_{R_i} and m_{T_i}, can be expressed as

$$f_{m_{\mathrm{R}_i}}(x) = \begin{cases} \frac{\theta(N_{\mathrm{R}})}{2\pi} & x = 1 \\ 1 - \frac{\theta(N_{\mathrm{R}})}{2\pi} & x = g(N_{\mathrm{R}}) \end{cases} \tag{28}$$

and

$$f_{m_{\mathrm{T}_i}}(x) = \begin{cases} \frac{\theta(N_{\mathrm{T}})}{2\pi} & x = 1 \\ 1 - \frac{\theta(N_{\mathrm{T}})}{2\pi} & x = g(N_{\mathrm{T}}) \end{cases}, \tag{29}$$

respectively.

From (26), (27), (28), and (29), antenna arrays with the same ρN value have the same directivity gain. Thus, ρN can be treated as a single factor in our following analysis.

C. Coverage Analysis

As discussed in Section II-A, the whole set of events that MS_0 is served by either an LOS BS or an NLOS BS can be denoted as $\mathcal{A}$. Furthermore, $\mathcal{A}$ can be divided into two disjoint subsets, $\mathcal{A}_{\mathrm{L}}$ and $\mathcal{A}_{\mathrm{N}}$, which are the sets of events that MS_0 is served by an LOS MS and an NLOS MS, respectively. Accordingly, the coverage probability P_{c} can be expressed as

$$\begin{aligned} P_{\mathrm{c}} &= P_{\mathcal{A}} \\ &= P_{\mathcal{A}_{\mathrm{L}}} + P_{\mathcal{A}_{\mathrm{N}}} \\ &= \int_0^{\infty} P_{\mathrm{c,L}}(x) f_{\mathrm{L}}(x)\,\mathrm{d}x + \int_0^{\infty} P_{\mathrm{c,N}}(x) f_{\mathrm{N}}(x)\,\mathrm{d}x \end{aligned} \tag{30}$$

where $f_{\mathrm{L}}(x)$ and $f_{\mathrm{N}}(x)$ are the PDFs given in Lemma 1, $P_{\mathrm{c,L}}(x)$ ($P_{\mathrm{c,N}}(x)$) is the conditional coverage probability given the condition that MS_0 is served by an LOS (NLOS) BS located at distance of x.

Theorem 1: If MS_0 is served by an LOS BS located at distance of x, the conditional coverage probability can be obtained by (31), shown at the bottom of this page. And if MS_0 is served by an NLOS BS located at distance of x, the conditional coverage probability can be obtained by (32), shown at the bottom of this page, where $s_{\mathrm{L}}(x) = \frac{T\beta_{\mathrm{L}}}{m_{\mathrm{R}_0} m_{\mathrm{T}_0} l_{\mathrm{L}}(x)}$, $s_{\mathrm{N}}(x) = \frac{T\beta_{\mathrm{N}}}{m_{\mathrm{R}_0} m_{\mathrm{T}_0} l_{\mathrm{N}}(x)}$, $\beta_{\mathrm{R}} = N_{\mathrm{R}}(N_{\mathrm{R}}!)^{-\frac{1}{N_{\mathrm{R}}}}$, $\beta_{\mathrm{T}} = N_{\mathrm{T}}(N_{\mathrm{T}}!)^{-\frac{1}{N_{\mathrm{T}}}}$, $\mathcal{L}_{I_{\mathrm{L,LOS}}}(s)$ and $\mathcal{L}_{I_{\mathrm{N,LOS}}}(s)$ ($\mathcal{L}_{I_{\mathrm{L,NLOS}}}(s)$ and $\mathcal{L}_{I_{\mathrm{N,NLOS}}}(s)$) are the Laplace transforms (LTs) of interference I_{L} and I_{N} with respect to s under the condition that MS_0 is served by an LOS (NLOS) BS, respectively.

Proof: The proof is given in Appendix B. ■

The LTs of $I_{\mathrm{L,LOS}}$, $I_{\mathrm{N,LOS}}$, $I_{\mathrm{L,NLOS}}$ and $I_{\mathrm{N,NLOS}}$ can be expressed as (33), (34), (35) and (36), respectively, shown at the bottom of the next page. The derivations are given in Appendix C.

Using (23), (24), (26)–(29), and (33)–(36), the coverage probability of MS_0 can be further derived in Theorem 2.

Theorem 2: In the mmWave cellular network with imperfect alignment, if MS_0 is served by the BS which provides the largest received signal power, the coverage probability P_{c} can be expressed as (37) in the bottom of the next page.

Proof: The proof is given in Appendix D. ■

1) Special Case: No-Blockage Regime with $\beta = 0$ and Full-Blockage Regime with $\beta = \infty$

In no-blockage regime (NBR) and full-blockage regime (FBR), all BSs are LOS and NLOS, respectively. Thus, there is only a single type of BSs in the whole mmWave networks. In the two extreme regimes, the serving BS of each MS which provides the largest received signal power is the nearest one in distance. Furthermore, we can obtain the coverage probabilities in these two extreme regimes from Corollary 1.

Corollary 1: In the mmWave cellular network with imperfect alignment, if MS_0 is served by the BS which provides the largest received signal power, the coverage probabilities P_{c}

$$P_{\mathrm{c,L}}(x) = \mathbb{E}_{m_{\mathrm{R}_0}, m_{\mathrm{T}_0}}\left[\sum_{n=1}^{N_{\mathrm{L}}} (-1)^{n+1} \binom{N_{\mathrm{L}}}{n} e^{-n s_{\mathrm{L}}(x)\sigma_n^2} \mathcal{L}_{I_{\mathrm{L,LOS}}}(n s_{\mathrm{L}}(x))\, \mathcal{L}_{I_{\mathrm{N,LOS}}}(n s_{\mathrm{L}}(x))\right], \tag{31}$$

$$P_{\mathrm{c,N}}(x) = \mathbb{E}_{m_{\mathrm{R}_0}, m_{\mathrm{T}_0}}\left[\sum_{n=1}^{N_{\mathrm{N}}} (-1)^{n+1} \binom{N_{\mathrm{N}}}{n} e^{-n s_{\mathrm{N}}(x)\sigma_n^2} \mathcal{L}_{I_{\mathrm{L,NLOS}}}(n s_{\mathrm{N}}(x))\, \mathcal{L}_{I_{\mathrm{N,NLOS}}}(n s_{\mathrm{N}}(x))\right] \tag{32}$$

for no-blockage regime and full-blockage regime can be calculated as (38) in the bottom of this page, where $\mathcal{L}_{I_{\rm s}}(s)$ is expressed in (39) in the bottom of this page. For NBF, $N_{\rm s} = N_{\rm L}$, $\beta_{\rm s} = \beta_{\rm L}$, $l_{\rm s}(x) = l_{\rm L}(x)$, and for FBR, $N_{\rm s} = N_{\rm N}$, $\beta_{\rm s} = \beta_{\rm N}$, $l_{\rm s}(x) = l_{\rm N}(x)$.

Proof: In Theorem 2, setting $\beta = 0$ or $\beta = \infty$, the coverage probability expression can be simplified as (38). ■

2) Special Case: Perfect Beam Alignment

If the antenna arrays at the MS side and its serving BS side are aligned perfectly, i.e., $\sigma_{\rm R} = \sigma_{\rm T} = 0$, the directivity gains for the desired signal achieve their maximum value, i.e., $m_{{\rm R}_0} = m_{{\rm T}_0} = 1$. We can further obtain Corollary 2.

Corollary 2: In the mmWave cellular network with perfect alignment, if MS_0 is served by the BS which provides the largest received signal power, the coverage probability $P_{\rm c}$ can be expressed as (40) in the bottom of this page.

Proof: The coverage probability with perfect beam alignment in (40) is obtained by substituting the constant directivity gains $m_{{\rm R}_0} = m_{{\rm T}_0} = 1$ into (37). ■

Remark 1: The coverage probability with perfect beam alignment in (40) is the same as the coverage probability expression in Theorem 1 of [15]. In other words, the coverage probability expression analyzed in [15] is a special case of our general coverage probability results in (37).

IV. NUMERICAL RESULTS

In this section, the impacts of alignment errors, the number of elements in the antenna array as well as the BS intensity on the system coverage probability will be discussed, and the accuracy of coverage probability expression will be verified. Without loss of generality, the mmWave cellular network is

$$\mathcal{L}_{I_{\rm L,LOS}}(s) = \exp\left(-2\pi\lambda\mathbb{E}_{m_{{\rm R}_i},m_{{\rm T}_i}}\left[\int_x^\infty\left(1-\left(\frac{1}{1+\frac{sl_{\rm L}(t)m_{{\rm R}_i}m_{{\rm T}_i}}{N_{\rm L}}}\right)^{N_{\rm L}}\right)t\mathbb{P}_{\rm LOS}(t)\,{\rm d}t\right]\right), \tag{33}$$

$$\mathcal{L}_{I_{\rm N,LOS}}(s) = \exp\left(-2\pi\lambda\mathbb{E}_{m_{{\rm R}_i},m_{{\rm T}_i}}\left[\int_{\psi_{\rm L}(x)}^\infty\left(1-\left(\frac{1}{1+\frac{sl_{\rm N}(t)m_{{\rm R}_i}m_{{\rm T}_i}}{N_{\rm N}}}\right)^{N_{\rm N}}\right)t\mathbb{P}_{\rm NLOS}(t)\,{\rm d}t\right]\right), \tag{34}$$

$$\mathcal{L}_{I_{\rm L,NLOS}}(s) = \exp\left(-2\pi\lambda\mathbb{E}_{m_{{\rm R}_i},m_{{\rm T}_i}}\left[\int_{\psi_{\rm N}(x)}^\infty\left(1-\left(\frac{1}{1+\frac{sl_{\rm L}(t)m_{{\rm R}_i}m_{{\rm T}_i}}{N_{\rm L}}}\right)^{N_{\rm L}}\right)t\mathbb{P}_{\rm LOS}(t)\,{\rm d}t\right]\right), \tag{35}$$

$$\mathcal{L}_{I_{\rm N,NLOS}}(s) = \exp\left(-2\pi\lambda\mathbb{E}_{m_{{\rm R}_i},m_{{\rm T}_i}}\left[\int_x^\infty\left(1-\left(\frac{1}{1+\frac{sl_{\rm N}(t)m_{{\rm R}_i}m_{{\rm T}_i}}{N_{\rm N}}}\right)^{N_{\rm N}}\right)t\mathbb{P}_{\rm NLOS}(t)\,{\rm d}t\right]\right), \tag{36}$$

$$\begin{aligned}P_{\rm c} = {} & \sum_{n=1}^{N_{\rm L}}(-1)^{n+1}\tbinom{N_{\rm L}}{n}\int_0^\infty f_{\rm L}(x)\,\mathbb{E}_{m_{{\rm R}_0},m_{{\rm T}_0}}\left[e^{-ns_{\rm L}(x)\sigma_n^2}\mathcal{L}_{I_{\rm L,LOS}}(ns_{\rm L}(x))\,\mathcal{L}_{I_{\rm N,LOS}}(ns_{\rm L}(x))\right]{\rm d}x\\ & +\sum_{n=1}^{N_{\rm N}}(-1)^{n+1}\tbinom{N_{\rm N}}{n}\int_0^\infty f_{\rm N}(x)\,\mathbb{E}_{m_{{\rm R}_0},m_{{\rm T}_0}}\left[e^{-ns_{\rm N}(x)\sigma_n^2}\mathcal{L}_{I_{\rm L,NLOS}}(ns_{\rm N}(x))\,\mathcal{L}_{I_{\rm N,NLOS}}(ns_{\rm N}(x))\right]{\rm d}x.\end{aligned} \tag{37}$$

$$P_{\rm c} = \sum_{n=1}^{N_{\rm s}}(-1)^{n+1}\tbinom{N_{\rm s}}{n}\int_0^\infty 2\pi\lambda xe^{-2\pi\lambda x^2}\mathbb{E}_{m_{{\rm R}_0},m_{{\rm T}_0}}\left[e^{-\frac{nT\beta_{\rm s}}{m_{{\rm R}_0}m_{{\rm T}_0}l_{\rm s}(x)}\sigma_n^2}\mathcal{L}_{I_{\rm s}}\left(\frac{nT\beta_{\rm s}}{m_{{\rm R}_0}m_{{\rm T}_0}l_{\rm s}(x)}\right)\right]{\rm d}x \tag{38}$$

$$\mathcal{L}_{I_{\rm s}}(s) = \exp\left(-2\pi\lambda\mathbb{E}_{m_{{\rm R}_i},m_{{\rm T}_i}}\left[\int_x^\infty\left(1-\left(\frac{1}{1+\frac{sl_{\rm s}(t)m_{{\rm R}_i}m_{{\rm T}_i}}{N_{\rm s}}}\right)^{N_{\rm s}}\right)t{\rm d}t\right]\right). \tag{39}$$

$$\begin{aligned}P_{\rm c} = {} & \sum_{n=1}^{N_{\rm L}}(-1)^{n+1}\tbinom{N_{\rm L}}{n}\int_0^\infty f_{\rm L}(x)\left[e^{-n\frac{T\beta_{\rm L}}{l_{\rm L}(x)}\sigma_n^2}\mathcal{L}_{I_{\rm L,LOS}}\left(n\frac{T\beta_{\rm L}}{l_{\rm L}(x)}\right)\mathcal{L}_{I_{\rm N,LOS}}\left(n\frac{T\beta_{\rm L}}{l_{\rm L}(x)}\right)\right]{\rm d}x\\ & +\sum_{n=1}^{N_{\rm N}}(-1)^{n+1}\tbinom{N_{\rm N}}{n}\int_0^\infty f_{\rm N}(x)\left[e^{-n\frac{T\beta_{\rm N}}{l_{\rm N}(x)}\sigma_n^2}\mathcal{L}_{I_{\rm L,NLOS}}\left(n\frac{T\beta_{\rm N}}{l_{\rm N}(x)}\right)\mathcal{L}_{I_{\rm N,NLOS}}\left(n\frac{T\beta_{\rm N}}{l_{\rm N}(x)}\right)\right]{\rm d}x.\end{aligned} \tag{40}$$

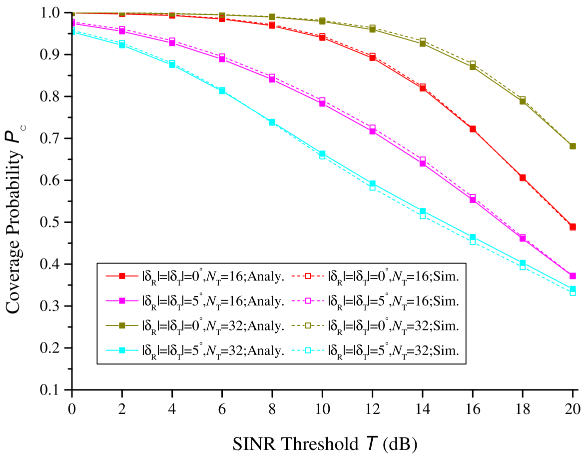

Fig. 4. Coverage probability versus T for $\lambda = \frac{1}{\pi} \times 10^{-4}\ m^{-2}$.

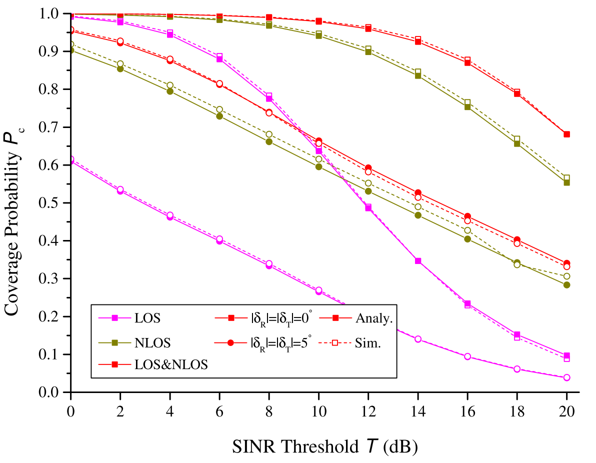

Fig. 5. Coverage probability Coverage probability versus T in different blockage regimes for $\lambda = \frac{1}{\pi} \times 10^{-4}\ m^{-2}$ and $N_T = 32$.

assumed to work in an environment with blockage parameter $\beta = 0.0069$ such that the BS at the distance of 100 meters can be LOS and NLOS with equal probability. Following the parameter setting in [15], we assume the mmWave network is operated at 28 GHz, and the bandwidth assigned to each user is 100 MHz. The noise power normalized by the transmit power is set to be -124 dB. The path loss exponents and Nakagami parameters are set to be $\alpha_L = 2\,(\alpha_N = 4)$ and $N_L = 3\,(N_N = 2)$ for LOS (NLOS) propagation paths, respectively. According to our prior analysis, systems with the same ρN value have the same coverage performance. Changing the element separation is equivalent to changing the number of elements in the antenna array. Thus, element separations of all antenna arrays are set to be a quarter of wavelength, i.e., $\rho = 1/4$ [21]. Due to the space limit of MS, the number of elements in the antenna array at MS is set to be $N_R = 8$.

Fig. 4 shows the coverage probability against the SINR threshold. The results indicate that the analytical expression is quite accurate to measure the system coverage probability. It can also be seen that when the MS and its serving BS are aligned perfectly, the system with lager antenna arrays has higher coverage probability. Moreover, beam alignment errors will impair the coverage performance significantly. More detailed results are given in the following.

Fig. 5 shows the coverage probability in different blockage regimes: general regime (GBR) with $\beta = 0.0069$, NBR with $\beta = 0$, and FBR with $\beta = \infty$ when $N_T = 32$. It can be seen that the coverage performance in general blockage environment where both LOS BSs and NLOS BSs exist outperforms the coverage in NBR and FBR. The reason is that in GBR the serving BS may be LOS one and interfering BSs are mostly NLOS ones. Thus, the desired power received by MS is high and the interfering power is relatively low, which results in high coverage probability. Meanwhile, the desired power in FBR propagating NLOS path is weaker and the interfering power in NBF propagating LOS path is stronger. Therefore, FBR and NBR achieve worse coverage performance. Moreover, there is a significant gap between the coverage probability in FBR and the coverage in FBR and GBR. The reason is that the interfering power from LOS BSs affects the performance severely. The interference in NBR is such strong that degrade the coverage performance significantly.

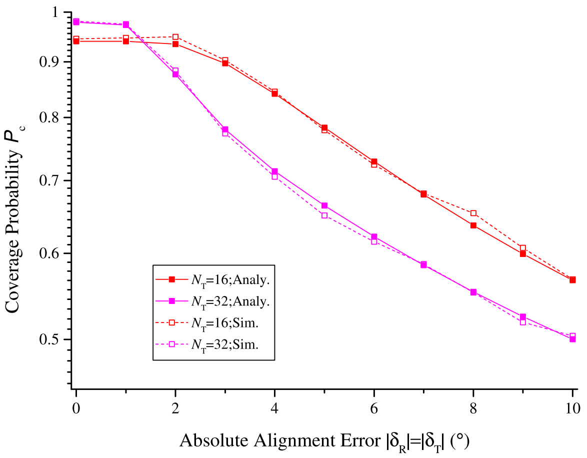

Fig. 6. Coverage probability versus $|\delta|$ with $\lambda = \frac{1}{\pi} \times 10^{-4}\ m^{-2}$, $|\delta_R| = |\delta_T| = |\delta|$, and $T = 10$ dB.

Fig. 6 provides the coverage probability with different beam alignment errors. It can be seen that the coverage probability decreases with the increase of alignment errors. Moreover, when the alignment error is relatively small, the decrease of the coverage probability is not remarkable. Particularly, it can be seen that the maxima of average absolute alignment errors without degrading the coverage performance are 2° and 1° for $N_T = 16$ and $N_T = 32$, respectively. This is because that when the average absolute alignment error is smaller than half of the mainlobe beamwidth, the misalignment occurs with low probability. It also can be seen that the coverage probability with $N_T = 32$ is lower than that with $N_T = 16$ when the beam alignment error is relatively high. This is because that when the alignment error is relatively high, the misalignment occurs with high probability. The narrow mainlobe beamwidth of large antenna array deteriorates the alignment, and the low sidelobe gain further decreases the desired signal power.

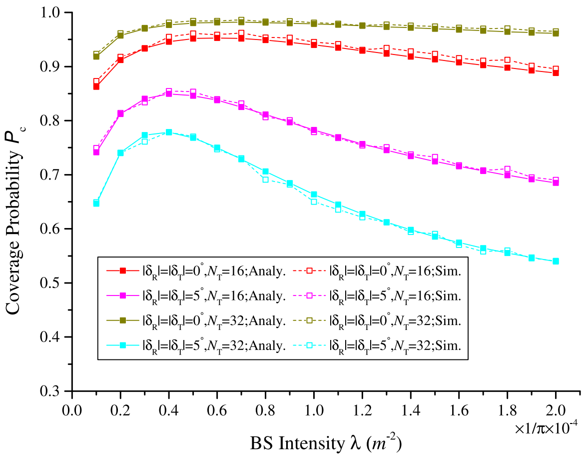

Fig. 7. Coverage probability versus λ for different beam alignment errors with $T = 10$ dB.

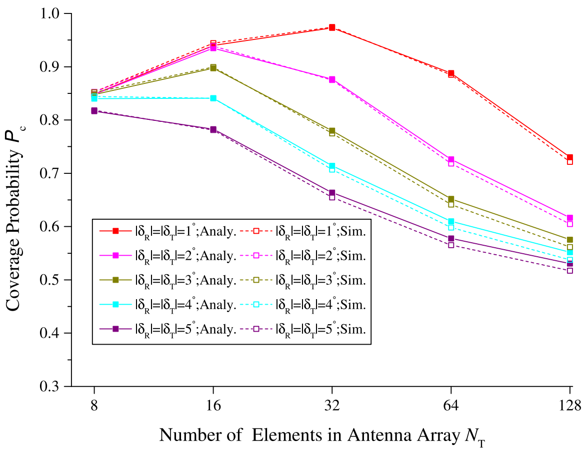

Fig. 8. Coverage probability versus N_T with $\lambda = \frac{1}{\pi} \times 10^{-4}\ m^{-2}$ for different beam alignment errors with $T = 10$ dB.

Fig. 7 shows the coverage probability versus BS intensity. It can be seen that when the BS density is low, the coverage probability is improved with the increase of the BS intensity. The reason is when the BS intensity is low, the distance between MS and its serving BS is large. Therefore, their propagation path is with high probability to be NLOS. Due to the high path loss of NLOS path, the receiving power of the desired signal is small and the coverage probability is low. By increasing the BS intensity, the distance between MS and its serving BS can be shortened and their propagation path may become LOS. Since the path loss is relatively low for LOS path, the coverage probability is improved with the increasing of receiving power of the desired signal. However, it should be noted that the increasing BS intensity cannot always improve the coverage probability, especially for the scenarios with beam alignment errors. When the BS intensity is high, the increase of BS intensity will shorten the distance between MS and its serving BS as well as the distances between MS and its interfering BSs. Both the desired and interfering signals are strengthened. In this case, if there is no beam alignment error, the coverage probability will decline with the increase of the BS intensity slightly due to the strengthened interference. But if the beam alignment error exists, the azimuth of BS may not fall in the mainlobe of the antenna array of MS and the azimuth of MS may fall in the sidelobe of the antenna array of BS. In this case, the beamforming gains cannot be exploited to improve the desired signals. On the contrary, since there are a lot of interfering BSs surrounding the typical MS, some interfering signals are strengthened unexpectedly. Therefore, when the BS intensity is high, the beam alignment errors will deteriorate the coverage probability significantly.

Fig. 8 shows the coverage probability with different number of elements in the antenna array. It can be seen that when the number of elements in the antenna array is small, the coverage probability can be improved by adding antenna elements. The reason is that the mainlobe beamwidth of small antenna array is wide enough to keep beam alignment. Therefore, interference power can be decreased by reducing the sidelobe gain of the antenna array. However, it should be noted that increasing the number of elements in the antenna array cannot always improve the coverage probability. It can be observed that when the number of elements in the antenna array grows larger and the alignment errors exist, the mainlobe beamwidth becomes too narrow to guarantee the beam alignment. Therefore, the coverage probability deteriorates significantly.

V. CONCLUSION

This paper has analyzed the coverage probability of mmWave celluar networks with imperfect beam alignment. Based on the enhanced flat-top antenna model for the mainlobe beamwidth and directivity gains of antenna arrays, we studied the impacts of number of elements in the antenna array and imperfect beam alignment by modeling the beam alignment errors as truncated Gaussian variables. The coverage probability has been derived in a tractable analytical expression. Simulation results have demonstrated the accuracy of our theoretical analysis. Under the practical constraints of imperfect beam alignment, our analytical expression can provide an optimal antenna arrays deployment scheme. Several important conclusions are drawn as follows.

- The coverage performance will not be deteriorated by small beam alignment errors. The robustness against the beam alignment errors depends on the number of elements in the antenna arrays. The mmWave cellular networks with less number of elements in the antenna arrays can remain high coverage performance with suffering from relatively larger beam alignment errors. In the scenarios such as strong wind occurs, perfect beam alignment is hard to realize. Smaller antenna arrays will provide better performance.
- The coverage probability is affected by the BS intensity. When the BS intensity is low, the increase of BS intensity will improve the coverage probability. However, when the BS intensity grows large, the coverage probability declines. The optimal BS intensity, which can be obtained through analysis, is of significance to direct the networks design and deployment.
- When the beam alignment errors are small enough, the coverage performance can be improved by increasing the

number of elements in the antenna array. However, when the beam alignment errors are large, the alignment probability of large antenna arrays may not be high enough such that increasing the number of elements in the antenna array will decrease the coverage probability. In practice, the optimal antenna arrays can be selected according to the beam alignment errors to obtain the best coverage performance.

APPENDIX A
PROOF OF LEMMA 1

If MS_0 is served by its nearest LOS BS at the distance of x, there are no LOS BSs in the circle with radius x and centre o, and there is at least one LOS BS in the annulus of circles with radii x and $x + \Delta x$ as $\Delta x \to 0$. Furthermore, there are no NLOS BS in the circle with radius $\psi_L(x + \Delta x)$ and centre o. Therefore, the probability that MS_0 is served by an LOS BS at distance of x can be obtained as (A.1) at the bottom of this page. Then, the PDF of the distance between MS_0 and its serving LOS BS can be obtained as (A.2) at the bottom of this page.

Similarly, the PDF of the distance between MS_0 and its serving NLOS BS can be derived as (A.3) at the bottom of this page.

APPENDIX B
PROOF OF THEOREM 1

If MS_0 is served by an LOS BS located at the distance of x, the received SINR at MS_0 is expressed in (B.1) at the bottom of this page. The conditional coverage probabilities $P_{\mathrm{c,L}}$ can be calculated as (B.2) at the bottom of this page, where (a) is from [33] and the independence between the directivity gains and the point process of the BSs, (b) follows the Binomial theorem and the assumption that N_{L} is an integer, (c) follows from the independence between the two point processes Φ_{L} and Φ_{N}, and (d) is from the definition of the Laplace transform.

$$P_{\mathrm{L}} = e^{-2\pi\lambda \int_0^x t\mathbb{P}_{\mathrm{LOS}}(t)\mathrm{d}t} \left(1 - e^{-2\pi\lambda \int_x^{x+\Delta x} t\mathbb{P}_{\mathrm{LOS}}(t)\mathrm{d}t}\right) e^{-2\pi\lambda \int_0^{\psi_L(x+\Delta x)} t\mathbb{P}_{\mathrm{NLOS}}(t)\mathrm{d}t}, \ x > 0, \ \Delta x \to 0. \tag{A.1}$$

$$\begin{aligned} f_{\mathrm{L}}(x) &= \lim_{\Delta x \to 0} \frac{P_{\mathrm{L}}}{\Delta x} \\ &= \lim_{\Delta x \to 0} \frac{e^{-2\pi\lambda \int_0^x t\mathbb{P}_{\mathrm{LOS}}(t)\mathrm{d}t} \left(2\pi\lambda x \mathbb{P}_{\mathrm{LOS}}(x) e^{-2\pi\lambda \int_0^{\psi_{\mathrm{L}}(x)} t\mathbb{P}_{\mathrm{NLOS}}(t)\mathrm{d}t} \cdot \Delta x + o\left((\Delta x)^2\right)\right)}{\Delta x} \\ &= 2\pi\lambda x \mathbb{P}_{\mathrm{LOS}}(x) e^{-2\pi\lambda\left(\int_0^x t\mathbb{P}_{\mathrm{LOS}}(t)\mathrm{d}t + \int_0^{\psi_{\mathrm{L}}(x)} t\mathbb{P}_{\mathrm{NLOS}}(t)\mathrm{d}t\right)}, \ x > 0. \end{aligned} \tag{A.2}$$

$$f_{\mathrm{N}}(x) = 2\pi\lambda x \mathbb{P}_{\mathrm{NLOS}}(x) e^{-2\pi\lambda\left(\int_0^x t\mathbb{P}_{\mathrm{NLOS}}(t)\mathrm{d}t + \int_0^{\psi_{\mathrm{L}}(x)} t\mathbb{P}_{\mathrm{LOS}}(t)\mathrm{d}t\right)}, \ x > 0 \tag{A.3}$$

$$\begin{aligned} \mathrm{SINR}_{\mathrm{L}} &= \frac{h_{\mathrm{L}0} m_{\mathrm{R}_0} m_{\mathrm{T}_0} l_{\mathrm{L}}(x)}{\sum_{i \in \Phi_{\mathrm{L}} \setminus b(o,x)} h_{\mathrm{L}i} m_{\mathrm{R}_i} m_{\mathrm{T}_i} l_{\mathrm{L}}(r_i) + \sum_{i \in \Phi_{\mathrm{N}} \setminus b(o,\psi_{\mathrm{L}}(x))} h_{\mathrm{N}i} m_{\mathrm{R}_i} m_{\mathrm{T}_i} l_{\mathrm{N}}(r_i) + \sigma_n^2} \\ &= \frac{h_{\mathrm{L}0} m_{\mathrm{R}_0} m_{\mathrm{T}_0} l_{\mathrm{L}}(x)}{I_{\mathrm{L,LOS}} + I_{\mathrm{N,LOS}} + \sigma_n^2}. \end{aligned} \tag{B.1}$$

$$\begin{aligned} P_{\mathrm{c,L}}(x) &= \mathbb{P}\left[\mathrm{SINR}_{\mathrm{L}} > T\right] \\ &= \mathbb{P}\left[\frac{h_{\mathrm{L}0} m_{\mathrm{R}_0} m_{\mathrm{T}_0} l_{\mathrm{L}}(x)}{I_{\mathrm{L,LOS}} + I_{\mathrm{N,LOS}} + \sigma_n^2} > T\right] \\ &= \mathbb{P}\left[h_{\mathrm{L}0} > \frac{T}{m_{\mathrm{R}_0} m_{\mathrm{T}_0} l_{\mathrm{L}}(x)}\left(I_{\mathrm{L,LOS}} + I_{\mathrm{N,LOS}} + \sigma_n^2\right)\right] \\ &\overset{(a)}{\approx} \mathbb{E}_{m_{\mathrm{R}_0}, m_{\mathrm{T}_0}}\left[1 - \mathbb{E}_{I_{\mathrm{L,LOS}}, I_{\mathrm{N,LOS}}}\left[\left(1 - e^{-\frac{T}{m_{\mathrm{R}_0} m_{\mathrm{T}_0} l_{\mathrm{L}}(x)}(x)\left(I_{\mathrm{L,LOS}} + I_{\mathrm{N,LOS}} + \sigma_n^2\right)}\right)^{N_{\mathrm{L}}}\right]\right] \\ &\overset{(b)}{=} \mathbb{E}_{m_{\mathrm{R}_0}, m_{\mathrm{T}_0}}\left[\sum_{n=1}^{N_{\mathrm{L}}} (-1)^{n+1} \binom{N_{\mathrm{L}}}{n} \mathbb{E}_{I_{\mathrm{L,LOS}}, I_{\mathrm{N,LOS}}}\left[e^{-n s_{\mathrm{L}}(x)\left(I_{\mathrm{L,LOS}} + I_{\mathrm{N,LOS}} + \sigma_n^2\right)}\right]\right] \\ &\overset{(c)}{=} \mathbb{E}_{m_{\mathrm{R}_0}, m_{\mathrm{T}_0}}\left[\sum_{n=1}^{N_{\mathrm{L}}} (-1)^{n+1} \binom{N_{\mathrm{L}}}{n} e^{-n s_{\mathrm{L}}(x)\sigma_n^2} \mathbb{E}_{I_{\mathrm{L,LOS}}}\left[e^{-n s_{\mathrm{L}}(x) I_{\mathrm{L,LOS}}}\right] \mathbb{E}_{I_{\mathrm{N,LOS}}}\left[e^{-n s_{\mathrm{L}}(x) I_{\mathrm{N,LOS}}}\right]\right] \\ &\overset{(d)}{=} \mathbb{E}_{m_{\mathrm{R}_0}, m_{\mathrm{T}_0}}\left[\sum_{n=1}^{N_{\mathrm{L}}} (-1)^{n+1} \binom{N_{\mathrm{L}}}{n} e^{-n s_{\mathrm{L}}(x)\sigma_n^2} \mathcal{L}_{I_{\mathrm{L,LOS}}}\left(n s_{\mathrm{L}}(x)\right) \mathcal{L}_{I_{\mathrm{N,LOS}}}\left(n s_{\mathrm{L}}(x)\right)\right] \end{aligned} \tag{B.2}$$

$$
\begin{aligned}
\mathrm{SINR}_{\mathrm{N}} &= \frac{h_{\mathrm{N}0} m_{\mathrm{R}_0} m_{\mathrm{T}_0} l_{\mathrm{N}}(x)}{\sum_{i \in \Phi_{\mathrm{L}} \setminus b(o,\psi_{\mathrm{N}}(x))} h_{\mathrm{L}i} m_{\mathrm{R}_i} m_{\mathrm{T}_i} l_{\mathrm{L}}(r_i) + \sum_{i \in \Phi_{\mathrm{N}} \setminus b(o,x)} h_{\mathrm{N}i} m_{\mathrm{R}_i} m_{\mathrm{T}_i} l_{\mathrm{N}}(r_i) + \sigma_n^2} \\
&= \frac{h_{\mathrm{N}0} m_{\mathrm{R}_0} m_{\mathrm{T}_0} l_{\mathrm{N}}(x)}{I_{\mathrm{L,NLOS}} + I_{\mathrm{N,NLOS}} + \sigma_n^2}.
\end{aligned} \tag{B.3}
$$

$$
P_{\mathrm{c,N}}(x) = \mathbb{E}_{m_{\mathrm{R}_0}, m_{\mathrm{T}_0}} \left[\sum_{n=1}^{N_{\mathrm{N}}} (-1)^{n+1} \binom{N_{\mathrm{N}}}{n} e^{-n s_{\mathrm{N}}(x) \sigma_n^2} \mathcal{L}_{I_{\mathrm{L,NLOS}}}(n s_{\mathrm{N}}(x)) \mathcal{L}_{I_{\mathrm{N,NLOS}}}(n s_{\mathrm{N}}(x)) \right]. \tag{B.4}
$$

$$
\begin{aligned}
\mathcal{L}_{I_{\mathrm{L,LOS}}}(s) &= \mathbb{E}\left[e^{-s I_{\mathrm{L,LOS}}}\right] \\
&= \mathbb{E}\left[e^{-s \sum_{i \in \Phi_{\mathrm{L}} \setminus b(o,x)} h_{\mathrm{L}i} m_{\mathrm{R}_i} m_{\mathrm{T}_i} l_{\mathrm{L}}(r_i)}\right] \\
&\overset{(a)}{=} \mathbb{E}\left[\prod_{i \in \Phi_{\mathrm{L}} \setminus b(o,x)} e^{-s h_{\mathrm{L}i} m_{\mathrm{R}_i} m_{\mathrm{T}_i} l_{\mathrm{L}}(r_i)}\right] \\
&\overset{(b)}{=} \exp\left(-2\pi\lambda \mathbb{E}_{m_{\mathrm{R}_i}, m_{\mathrm{T}_i}}\left[\int_x^\infty \left(1 - \mathbb{E}_{h_{\mathrm{L}}}\left[e^{-s l_{\mathrm{L}}(t) h_{\mathrm{L}} m_{\mathrm{R}_i} m_{\mathrm{T}_i}}\right]\right) t \mathbb{P}_{\mathrm{LOS}}(t)\, \mathrm{d}t\right]\right) \\
&\overset{(c)}{=} \exp\left(-2\pi\lambda \mathbb{E}_{m_{\mathrm{R}_i}, m_{\mathrm{T}_i}}\left[\int_x^\infty \left(1 - \left(\frac{1}{1 + \frac{s l_{\mathrm{L}}(t) m_{\mathrm{R}_i} m_{\mathrm{T}_i}}{N_{\mathrm{L}}}}\right)^{N_{\mathrm{L}}}\right) t \mathbb{P}_{\mathrm{LOS}}(t)\, \mathrm{d}t\right]\right)
\end{aligned} \tag{C.1}
$$

$$
\begin{aligned}
P_{\mathrm{c}} &= \int_0^\infty \mathbb{E}_{m_{\mathrm{R}_0}, m_{\mathrm{T}_0}}\left[\sum_{n=1}^{N_{\mathrm{L}}} (-1)^{n+1} \binom{N_{\mathrm{L}}}{n} e^{-n s_{\mathrm{L}}(x) \sigma_n^2} \mathcal{L}_{I_{\mathrm{L,LOS}}}(n s_{\mathrm{L}}(x)) \mathcal{L}_{I_{\mathrm{N,LOS}}}(n s_{\mathrm{L}}(x))\right] f_{\mathrm{L}}(x)\, \mathrm{d}x \\
&\quad + \int_0^\infty \mathbb{E}_{m_{\mathrm{R}_0}, m_{\mathrm{T}_0}}\left[\sum_{n=1}^{N_{\mathrm{N}}} (-1)^{n+1} \binom{N_{\mathrm{N}}}{n} e^{-n s_{\mathrm{N}}(x) \sigma_n^2} \mathcal{L}_{I_{\mathrm{L,NLOS}}}(n s_{\mathrm{N}}(x)) \mathcal{L}_{I_{\mathrm{N,NLOS}}}(n s_{\mathrm{N}}(x))\right] f_{\mathrm{N}}(x)\, \mathrm{d}x \\
&\overset{(a)}{=} \sum_{n=1}^{N_{\mathrm{L}}} (-1)^{n+1} \binom{N_{\mathrm{L}}}{n} \int_0^\infty f_{\mathrm{L}}(x) \mathbb{E}_{m_{\mathrm{R}_0}, m_{\mathrm{T}_0}}\left[e^{-n s_{\mathrm{L}}(x) \sigma_n^2} \mathcal{L}_{I_{\mathrm{L,LOS}}}(n s_{\mathrm{L}}(x)) \mathcal{L}_{I_{\mathrm{N,LOS}}}(n s_{\mathrm{L}}(x))\right] \mathrm{d}x \\
&\quad + \sum_{n=1}^{N_{\mathrm{N}}} (-1)^{n+1} \binom{N_{\mathrm{N}}}{n} \int_0^\infty f_{\mathrm{N}}(x) \mathbb{E}_{m_{\mathrm{R}_0}, m_{\mathrm{T}_0}}\left[e^{-n s_{\mathrm{N}}(x) \sigma_n^2} \mathcal{L}_{I_{\mathrm{L,NLOS}}}(n s_{\mathrm{N}}(x)) \mathcal{L}_{I_{\mathrm{N,NLOS}}}(n s_{\mathrm{N}}(x))\right] \mathrm{d}x
\end{aligned} \tag{D.1}
$$

Similarly, given MS_0 is served by an NLOS located at the distance of x, the received SINR at MS_0 is expressed in (B.3) at the top of this page. Further, the conditional coverage probabilities $P_{\mathrm{c,N}}$ can be derived as (B.4) at the top of this page.

APPENDIX C
DERIVATIONS OF (33)–(36)

The LT of $I_{\mathrm{L,LOS}}$ in (33) can be calculated as (C.1) at the top of this page, where (a) follows the independence between different interfering LOS propagation paths, (b) follows the probability generating functional (PGFL) of the PPP [34], and (c) is by computing the moment generating function of a gamma random variable h_{L}. The derivations of $\mathcal{L}_{I_{\mathrm{N,LOS}}}(s)$, $\mathcal{L}_{I_{\mathrm{L,NLOS}}}(s)$ and $\mathcal{L}_{I_{\mathrm{N,NLOS}}}(s)$ are in similar manner to $\mathcal{L}_{I_{\mathrm{L,LOS}}}(s)$ and so are omitted.

APPENDIX D
PROOF OF THEOREM 2

Substituting (31) and (32) into (30), we can get the coverage probability expressed as (D.1) at the top of this page, where step (a) is obtained by changing the order of the integer and the summation.

REFERENCES

[1] J. G. Andrews *et al.*, “What will 5G be?” *IEEE J. Sel. Areas Commun.*, vol. 32, no. 6, pp. 1065–1082, Jun. 2014.

[2] A. Osseiran, “Scenarios for 5G mobile and wireless communications: The vision of the METIS project,” *IEEE Commun. Mag.*, vol. 52, no. 5, pp. 26–35, May 2014.

[3] C. X. Wang *et al.*, “Cellular architecture and key technologies for 5G wireless communication networks,” *IEEE Commun. Mag.*, vol. 52, no. 2, pp. 122–130, Feb. 2014.

[4] Z. Pi and F. Khan, "An introduction to millimeter-wave mobile broadband systems," *IEEE Commun. Mag.*, vol. 49, no. 6, pp. 101–107, Jun. 2011.

[5] T. S. Rappaport *et al.*, "Millimeter wave mobile communications for 5G cellular: It will work!" *IEEE Access*, vol. 1, pp. 335–349, 2013.

[6] *High Rate Ultra Wideband PHY and MAC Standard*, Standard ECMA-368, 2008.

[7] *IEEE Standard for Information Technology—Local and Metropolitan Area networks–Specific Requirements–Part 15.3: Amendment 2: Millimeter-Wave-Based Alternative Physical Layer Extension*, IEEE Std 802.15.3c-2009 (Amendment to IEEE Std 802.15.3–2003), Oct. 2009.

[8] *ISO/IEC/IEEE International Standard for Information Technology–Telecommunications and Information Exchange Between Systems–Local and Metropolitan Area Networks—Specific Requirements—Part 11: Wireless LAN Medium Access Control (MAC) and Physical Layer (PHY) Specifications Amendment 3: Enhancements for Very High Throughput in the 60 GHz Band (Adoption of IEEE Std 802.11ad-2012)*, ISO/IEC/IEEE 8802–11:2012/Amd.3:2014(E), Mar. 2014.

[9] Y. P. Zhang, P. Wang, and A. Goldsmith, "Rainfall effect on the performance of millimeter-wave MIMO systems," *IEEE Trans. Wireless Commun.*, vol. 14, no. 9, pp. 4857–4866, Sep. 2015.

[10] S. Rajagopal, S. Abu-Surra , and M. Malmirchegini, "Channel feasibility for outdoor Non-line-of-sight mmWave mobile communication," in *Proc. IEEE Veh. Technol. Conf. Fall*, Québec City, QC, Canada, Sep. 2012, pp. 1–6.

[11] T. S. Rappaport, F. Gutierrez, E. Ben-Dor , J. N. Murdock, Y. Qiao, and J. I. Tamir, "Broadband millimeter-wave propagation measurements and models using adaptive-beam antennas for outdoor urban cellular communications," *IEEE Trans. Antennas Propag.*, vol. 61, no. 4, pp. 1850–1859, Apr. 2013.

[12] M. R. Akdeniz *et al.*, "Millimeter wave channel modeling and cellular capacity evaluation," *IEEE J. Sel. Areas Commun.*, vol. 32, no. 6, pp. 1164–1179, Jun. 2014.

[13] F. Baccelli and B. Błszczyszyn, "Stochastic geometry and wireless networks: Volume I theory," *Found. Trends Netw.*, vol. 3, no. 1/2, pp. 249–449, 2010. [Online]. Available: http://dx.doi.org/10.1561/1300000006

[14] J. G. Andrews, F. Baccelli, and R. K. Ganti, "A tractable approach to coverage and rate in cellular networks," *IEEE Trans. Commun.*, vol. 59, no. 11, pp. 3122–3134, Nov. 2011.

[15] T. Bai and R. W. Heath, "Coverage and rate analysis for millimeter-wave cellular networks," *IEEE Trans. Wireless Commun.*, vol. 14, no. 2, pp. 1100–1114, Feb. 2015.

[16] S. Singh, M. N. Kulkarni, A. Ghosh, and J. G. Andrews, "Tractable model for rate in self-backhauled millimeter wave cellular networks," *IEEE J. Sel. Areas Commun.*, vol. 33, no. 10, pp. 2196–2211, Oct. 2015.

[17] H. Elshaer, M. N. Kulkarni, F. Boccardi, J. G. Andrews, and M. Dohler, "Downlink and uplink cell association with traditional macrocells and millimeter wave small cells," *IEEE Trans. Wireless Commun.*, vol. 15, no. 9, pp. 6244–6258, Sep. 2016.

[18] L. Wang, K.-K. Wong, R. W. Heath, and J. Yuan, "Wireless powered dense cellular metworks: How many small cells do we need?" *IEEE J. Sel. Areas Commun.*, vol. 35, no. 9, pp. 2010–2024, Sep. 2017.

[19] A. Thornburg, T. Bai, and R. W. Heath, "Performance analysis of outdoor mmWave ad hoc networks," *IEEE Trans. Signal Process.*, vol. 64, no. 15, pp. 4065–4079, Aug. 2016.

[20] Y. Zhu, L. Wang, K.-K. Wong, and R. W. Heath, "Secure communications in millimeter wave ad hoc networks," *IEEE Trans. Wireless Commun.*, vol. 16, no. 5, pp. 3205–3217, May 2017.

[21] X. Yu, J. Zhang, M. Haenggi, and K. B. Letaief, "Coverage analysis for millimeter wave networks: The impact of directional antenna arrays," *IEEE J. Sel. Areas Commun.*, vol. 35, no. 7, pp. 1498–1512, Jul. 2017.

[22] D. Maamari, N. Devroye, and D. Tuninetti, "Coverage in mmWave cellular networks with base station co-operation," *IEEE Trans. Wireless Commun.*, vol. 15, no. 4, pp. 2981–2994, Apr. 2016.

[23] A. Thornburg and R. W. Heath, "Ergodic capacity in mmWave ad hoc network with imperfect beam alignment," in *Proc. IEEE Mil. Commun. Conf.*, Tampa, FL, USA, Oct. 2015, pp. 1479–1484.

[24] M. D. Renzo, "Stochastic geometry modeling and analysis of multi-tier millimeter wave cellular networks," *IEEE Trans. Wireless Commun.*, vol. 14, no. 9, pp. 5038–5057, Sep. 2015.

[25] M. Cheng *et al.*, "Coverage analysis for millimeter wave cellular networks with beam alignment errors," in *Proc IEEE Globecom Workshops*, Dec. 2017, pp. 1–6.

[26] T. Bai, R. Vaze, and R. W. Heath, "Analysis of blockage effects on urban cellular networks," *IEEE Trans. Wireless Commun.*, vol. 13, no. 9, pp. 5070–5083, Sep. 2014.

[27] J. G. Andrews, T. Bai, M. N. Kulkarni, A. Alkhateeb, A. K. Gupta, and R. W. Heath, "Modeling and analyzing millimeter wave cellular systems," *IEEE Trans. Commun.*, vol. 65, no. 1, pp. 403–430, Jan. 2017.

[28] A. M. Hunter, J. G. Andrews, and S. Weber, "Transmission capacity of ad hoc networks with spatial diversity," *IEEE Trans. Wireless Commun.*, vol. 7, no. 12, pp. 5058–5071, Dec. 2008.

[29] C. A. Balanis, *Antenna Theory: Analysis and Design, 4th ed*. Hoboken, NJ, USA: Wiley, 2016.

[30] V. Raghavan, J. Cezanne, S. Subramanian, A. Sampath, and O. Koymen, "Beamforming tradeoffs for initial ue discovery in millimeter-wave MIMO systems," *IEEE J. Sel. Topics Signal Process.*, vol. 10, no. 3, pp. 543–559, Apr. 2016.

[31] D. Zhu, J. Choi, and R. W. Heath, "Auxiliary beam pair enabled AoD and AoA estimation in closed-Loop large-scale millimeter-wave MIMO systems," *IEEE Trans. Wireless Commun.*, vol. 16, no. 7, pp. 4770–4785, Jul. 2017.

[32] J. Yu, Y.-D. Yao, A. F. Molisch, and J. Zhang, "Performance evaluation of CDMA reverse links with imperfect beamforming in a multicell environment using a simplified beamforming model," *IEEE Trans. Veh. Tech.*, vol. 55, no. 3, pp. 1019–1031, May 2006.

[33] H. Alzer, "Some inequalities for the incomplete Gamma function," *Math. Comput.*, vol. 66, no. 218, pp. 771–778, 1997. [Online]. Available: http://www.jstor.org/stable/2153894

[34] S. Mukherjee, *Analytical Modeling of Heterogeneous Cellular Networks: Geometry, Coverage, and Capacity*. Cambridge, U.K.: Cambridge Univ. Press, 2014.

Ming Cheng (S'17) received the B.S. degree in information engineering and the M.S. degree in communications engineering from Nanjing University of Aeronautics and Astronautics, Nanjing, China, in 2012 and 2015, respectively. He is currently working toward the Ph.D. degree with the National Mobile Communications Research Laboratory, Southeast University, Nanjing, China. His current research interests include applications of stochastic geometry, cloud radio access networks, mmWave communications, and massive MIMO.

Jun-Bo Wang (M'11) received the B.S. degree in computer science from Hefei University of Technology, Hefei, China, in 2003, and the Ph.D. degree in communications engineering from Southeast University, Nanjing, China, in 2008. From 2008 to 2013, he was with Nanjing University of Aeronautics and Astronautics. From 2011 to 2013, he was a Postdoctoral Fellow with the National Laboratory for Information Science and Technology, Tsinghua University, Beijing, China. He is currently an Associate Professor with the National Mobile Communications Research Laboratory, Southeast University. Since 2016, he has held a European Commission Marie Curie Fellowship and has been a Research Fellow with the University of Kent, United Kingdom. His current research interests are cloud radio access networks, mmWave communications, and wireless optical communications.

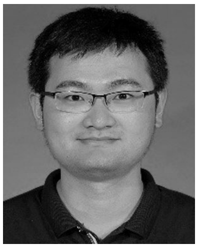

Yongpeng Wu (S'08–M'13–SM'17) received the B.S. degree in telecommunication engineering from Wuhan University, Wuhan, China, in July 2007, the Ph.D. degree in communication and signal processing with the National Mobile Communications Research Laboratory, Southeast University, Nanjing, China, in November 2013.

He is currently a Tenure-Track Associate Professor with the Department of Electronic Engineering, Shanghai Jiao Tong University, Shanghai, China. Previously, he was a Senior Research Fellow with Institute for Communications Engineering, Technical University of Munich, Munich, Germany and the Humboldt Research Fellow and the Senior Research Fellow with Institute for Digital Communications, University Erlangen-Nürnberg, Erlangen, Germany. During his doctoral studies, he conducted collaborative research with the Department of Electrical Engineering, Missouri University of Science and Technology, Rolla, MO, USA. His research interests include massive MIMO/MIMO systems, physical layer security, signal processing for wireless communications, and multivariate statistical theory.

Dr. Wu was awarded the IEEE Student Travel Grant for IEEE International Conference on Communications (ICC) 2010, the Alexander von Humboldt Fellowship in 2014, the Travel Grant for the IEEE Communication Theory Workshop 2016, the Excellent Doctoral Thesis Award of China Communications Society 2016, and the Excellent Editor Award of the IEEE COMMUNICATIONS LETTERS 2017. He was an Exemplary Reviewer of the IEEE TRANSACTIONS ON COMMUNICATIONS in 2015 and 2016. He is the lead Guest Editor for the special issue "Physical Layer Security for 5G Wireless Networks" of the IEEE JOURNAL ON SELECTED AREAS IN COMMUNICATIONS. He is currently an Editor of the IEEE ACCESS and the IEEE COMMUNICATIONS LETTERS. He has been a TPC member of various conferences, including Globecom, ICC, VTC, and PIMRC, etc.

Xiang-Gen Xia (M'97–S'00–F'09) received the B.S. degree in mathematics from Nanjing Normal University, Nanjing, China, and the M.S. degree in mathematics from Nankai University, Tianjin, China, and the Ph.D. degree in electrical engineering from the University of Southern California, Los Angeles, CA, USA, in 1983, 1986, and 1992, respectively.

He was a Senior/Research Staff Member with the Hughes Research Laboratories, Malibu, CA, USA, during 1995–1996. In September 1996, he was with the Department of Electrical and Computer Engineering, University of Delaware, Newark, DE, USA, where he is the Charles Black Evans Professor. He is the author of the book *Modulated Coding for Intersymbol Interference Channels* (New York, Marcel Dekker, 2000). His current research interests include space-time coding, MIMO and OFDM systems, digital signal processing, and SAR and ISAR imaging.

Dr. Xia was the recipient of the National Science Foundation (NSF) Faculty Early Career Development (CAREER) Program Award in 1997, the Office of Naval Research (ONR) Young Investigator Award in 1998, and the Outstanding Overseas Young Investigator Award from the National Nature Science Foundation of China in 2001. He is currently serving and has served as an Associate Editor for numerous international journals including the IEEE WIRELESS COMMUNICATIONS LETTERS, the IEEE TRANSACTIONS ON SIGNAL PROCESSING, the IEEE TRANSACTIONS ON WIRELESS COMMUNICATIONS, the IEEE TRANSACTIONS ON MOBILE COMPUTING, and the IEEE TRANSACTIONS ON VEHICULAR TECHNOLOGY. He is the Technical Program Chair of the Signal Processing Symp., Globecom 2007 in Washington D.C. and the General Co-Chair of ICASSP 2005 in Philadelphia.

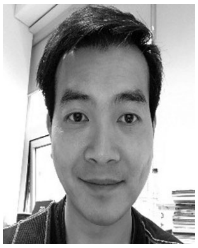

Kai-Kit Wong (M'01–SM'08–F'16) received the B.Eng., M.Phil., and Ph.D. degrees all in electrical and electronic engineering, from the Hong Kong University of Science and Technology, Hong Kong, in 1996, 1998, and 2001, respectively. After graduation, he took up academic and research positions with the University of Hong Kong, Lucent Technologies, Bell-Labs, Holmdel, the Smart Antennas Research Group of Stanford University, and the University of Hull, Hull, UK. He is the Chair in Wireless Communications with the Department of Electronic and Electrical Engineering, University College London, London, U.K. His current research centers around 5G and beyond mobile communications, including topics such as massive MIMO, full-duplex communications, millimetre-wave communications, edge caching and fog networking, physical layer security, wireless power transfer and mobile computing, V2X communications, and of course cognitive radios. There are also a few other unconventional research topics that he has set his heart on, including for example, fluid antenna communications systems, remote ECG detection and etc.

He is a co-recipient of the 2013 IEEE SIGNAL PROCESSING LETTERS Best Paper Award and the 2000 IEEE VTS Japan Chapter Award at the IEEE Vehicular Technology Conference in Japan in 2000, and a few other international best paper awards.

He is Fellow of IET and is also on the editorial board of several international journals. He has been a Senior Editor for the IEEE COMMUNICATIONS LETTERS since 2012 and also for the IEEE WIRELESS COMMUNICATIONS LETTERS since 2016. He was also an Associate Editor for the IEEE SIGNAL PROCESSING LETTERS from 2009 to 2012 and Editor for the IEEE TRANSACTIONS ON WIRELESS COMMUNICATIONS from 2005 to 2011. He was also a Guest Editor for the IEEE JSAC SI on virtual MIMO in 2013 and currently Guest Editor for IEEE JSAC SI on physical layer security for 5G.

Min Lin (M'13) received the B.S. degree from the National University of Defense Technology, Changsha, China, in 1993, the M.S. degree from the Nanjing Institute of Communication Engineering, Nanjing, China, in 2000, and the Ph.D. degree from Southeast University, Nanjing, China, in 2008, all in electrical engineering. He is a Professor with Nanjing University of Posts and Telecommunications, Nanjing, China. He has authored or co-authored more than 100 papers. His current research interests include wireless communications and array signal processing. He was the TPC member of many IEEE sponsored conferences, including ICC, Globecom, etc.